buildings

MDPI

Article

Performance Evaluation of Thermal Insulation Rubberized Mortar Modified by Fly Ash and Glass Fiber

Zezhou Pan [1], Feng Liu [1,*], Huawei Li [1], Xiaohui Li [1], Daochu Wang [2], Zao Ling [2], Huanyu Zhu [1] and Yuhao Zhu [1]

[1] School of Civil and Transportation Engineering, Guangdong University of Technology, Guangzhou 510006, China; 3121003163@mail2.gdut.edu.cn (Z.P.); 1122309001@mail2.gdut.edu.cn (H.L.); lixh@mail2.gdut.edu.cn (X.L.); 3121002912@mail2.gdut.edu.cn (H.Z.); zhuyh202009@163.com (Y.Z.)
[2] Guangzhou Construction Engineering Co., Ltd., Guangzhou 510180, China; wangdc202312@163.com (D.W.); lingz202106@163.com (Z.L.)
* Correspondence: fliu@gdut.edu.cn

Abstract: The utilization of waste rubber as a viable option for manufacturing building materials holds great significance for the sustainable development of the construction industry. This study explores the addition of two additives, fly ash (FA) and glass fiber (GF), to rubberized mortar in order to improve its performance. The impact of different waste rubber powder (RP) replacement rates and modified additive dosages on the performance of rubberized mortar, including fluidity, mechanical properties, drying shrinkage, impact resistance, and thermal insulation properties, was investigated. Furthermore, the analytic hierarchy process (AHP) was adopted to study the priorities of the rubberized mortar modified by FA and GF. The results indicate that the addition of RP leads to a decrease in mortar fluidity, mechanical properties, and drying shrinkage. However, it can enhance its impact resistance and thermal insulation properties. The additives, FA and GF, have a significant influence on the properties of rubberized mortar. By means of AHP method analysis, this study concludes that the optimal comprehensive properties of FA- and GF-modified rubberized mortar can be achieved by replacing 10% of sand with RP and using 10% FA and 0.4% GF. This study presents a configuration method for modified thermal insulation rubberized mortar, and it may lead to FA and GF being considered potential candidates for developing environmentally friendly building materials.

Keywords: rubberized mortar; waste rubber powder; fly ash; glass fiber; analytic hierarchy process; environmentally friendly building material

Citation: Pan, Z.; Liu, F.; Li, H.; Li, X.; Wang, D.; Ling, Z.; Zhu, H.; Zhu, Y. Performance Evaluation of Thermal Insulation Rubberized Mortar Modified by Fly Ash and Glass Fiber. *Buildings* **2024**, *14*, 221. https://doi.org/10.3390/buildings14010221

Academic Editor: Grzegorz Ludwik Golewski

Received: 6 December 2023
Revised: 9 January 2024
Accepted: 12 January 2024
Published: 14 January 2024

1. Introduction

The rapid growth of the automobile industry has resulted in a higher demand for tires [1,2]. Especially for emerging countries, growing income levels are driving the expansion of vehicle usage. As a consequence, the demand for tires is also on the rise [3]. It is estimated that approximately 1 billion tires are discarded each year, with a recycling rate of less than 50% [4]. At present, the options for disposing waste tires are limited, and one of the most commonly used methods is landfilling [4,5]. However, this approach requires a significant amount of land and poses a threat to groundwater resources in the landfill area. Moreover, the accumulation of discarded tires creates a breeding ground for mosquitoes, leading to potential health risks. Furthermore, discarded tires are highly susceptible to fires, which are notoriously difficult and costly to extinguish [6]. Thus, legislation has been introduced in many countries to restrict the disposal of waste tires in landfills and promote their reuse in other applications [3].

The construction industry is currently grappling with a shortage of natural resources, such as natural river sand, thus highlighting the need to prioritize sustainability [7,8]. One promising solution is the incorporation of waste tire rubber in the manufacturing of mortar and concrete, providing an environmentally friendly and sustainable approach to waste

disposal [9,10]. In recent years, numerous researchers have explored the potential of utilizing waste tire rubber as a partial replacement for natural fine aggregate in mortar [11,12]. They have discovered that waste tire rubber can be processed into rubber powder (RP) through mechanical grinding, which can then be used in the preparation of rubberized cement-based materials. However, recent studies on rubberized mortar have highlighted a possible decrease in mechanical properties, such as compressive and flexural strengths, due to the low elastic modulus of RP and the weak bonding interface between RP and cement paste [13,14]. Despite these limitations, the elastic nature of RP offers advantages in terms of energy absorption, toughness, deformation ability, high damping, and anti-fatigue ability. As a result, it helps to minimize the brittle failure behavior typically observed in traditional mortar and concrete [15,16].

In the sustainable design of buildings, it is crucial to consider energy consumption [17]. Energy conservation in buildings encompasses various aspects such as energy consumption for building heating, air conditioning, lighting, and more. The main objective is to enhance energy efficiency while ensuring the comfort of people's lives. One way to achieve this is by improving the thermal insulation properties of building materials, which helps minimize energy dissipation. Relevant research suggests that rubber has a notably lower thermal conductivity compared to cement mortar [18,19]. This characteristic makes rubber a promising option for thermal insulation mortar. Mostofinejad et al. [20] conducted a thermal characteristics test on rubber aggregate combined with silica fume concrete. Their findings indicate that rubber particles can be utilized for thermal insulation, and fine rubber particles have a greater impact on reducing the thermal conductivity of concrete compared to coarse rubber particles. Wang et al. [21] prepared recycled aggregate crumb rubber concrete (RCC) using recycled aggregate and rubber as raw materials. The results showed that RCC had excellent thermal performance. The thermal resistance increased significantly when the replacement rate of rubber material to replace sand reached 20%. Therefore, the application of waste rubber to the field of low-energy-consumption buildings holds great promise.

Although the addition of RP can enhance certain properties of mortar or concrete and provide environmental benefits, its practical engineering application still faces limitations. This is primarily due to the lack of understanding regarding the "functional design" of such cement-based materials and the need for a comprehensive evaluation of multiple properties. For instance, the workability of rubberized cement-based materials must be taken into consideration to ensure ease of construction [22]. In addition to different environmental humidity levels, the drying shrinkage of building materials should also be taken into account. In some use environments, building materials may not necessarily require high mechanical properties to meet engineering requirements. Additionally, in specific structural engineering applications, building materials may need to withstand vibration, explosion, and impact loads. As a result, the deformation and impact resistance of building materials should also be taken into consideration [23,24]. Therefore, it is important to consider and evaluate various properties of building materials in order to select those with excellent overall performances for specific engineering environments.

To enhance specific properties of rubberized cement-based materials, incorporating additives is a direct and straightforward approach [25–27]. Fly ash (FA), a common industrial by-product, possesses smooth morphological characteristics that facilitate a beneficial "ball-bearing effect". This effect effectively enhances the interfacial behavior between the slurry and aggregate [28,29]. Additionally, FA contributes to the mechanical properties of cement-based materials. Shao et al. [30] conducted a study using FA and crumb rubber to prepare ultra-high-performance concrete (UHPC), and their results demonstrated the significant impact of FA on the flexural properties of UHPC. Similar observations were found in studies conducted by Zhao et al. and Shao et al. [31,32]. Furthermore, these researchers suggested that FA also aids in improving the ductility of cement-based materials.

The addition of fiber materials is considered an effective method to enhance the mechanical properties and deformation resistance of rubberized cement-based materi-

als [33,34]. Yang et al. [35] conducted an experimental study on the compression–shear performance of steel fiber-reinforced rubber concrete. The results demonstrated that the combination of steel fiber and rubber exhibits a good synergistic effect, leading to the improved shear deformation toughness performance of rubber concrete. Xiong et al. [36] used a carbon fiber-reinforced polymer to prepare rubber concrete. The results show that the compressive strength of hybrid composites increases slightly, while the ductility, flexural toughness, impact resistance, and energy absorption capacity increase significantly. Su et al. [37] conducted a study on the preparation of basalt–polypropylene fiber-reinforced rubber concrete. The findings demonstrated that incorporating basalt and polypropylene fibers into rubber concrete leads to enhanced performance, particularly at higher temperatures. Glass fiber (GF) is an inorganic non-metallic material known for its insulation properties, heat resistance, tensile strength, and decay resistance [38,39]. These characteristics have made GF widely utilized in the field of constructional engineering. However, there is limited research available on the performance of glass-fiber-modified rubberized cement-based materials. Therefore, further research in this area is necessary to advance our understanding.

The objective of this work is to develop a rubberized mortar with superior comprehensive properties, including workability, mechanical properties, drying shrinkage, impact resistance, and thermal insulation properties. To achieve this, two additives, namely FA and GF, were incorporated into the rubberized mortar. This research examined the influence of RP replacement rate and FA and GF content on various specific properties of the mortar and investigated the underlying mechanisms. A representative test group was selected for evaluation of the thermal insulation properties. Additionally, the analytic hierarchy process (AHP) was utilized to determine the most suitable mix ratio for the representative test group. The findings of this study propose a configuration method for rubberized mortar with exceptional comprehensive properties, and these results are expected to contribute to the development of a new environmentally friendly building material for actual engineering projects.

2. Materials and Methods

2.1. Materials

Portland slag cement, according to the Chinese standard GB 1334-1999 [40], P.S.A 32.5, was used in this study, and its chemical composition and basic physical properties are displayed in Tables 1 and 2, respectively. The density of P.S.A 32.5 was measured according to the Chinese standard GB/T 208-2014 [41], and the setting time and flexural and compressive strength were measured according to GB/T 175-1999 [42]. RP was obtained from waste tires (with a particle size of 20 mesh) by grinding, and its density measures at 988 g/cm^3. Alkali-resistant GF was produced by Taishan Glass Fiber Co., Ltd.(Taian, China), and its physical parameters were obtained from the measurement of the company, as shown in Table 3. First-class FA used in this study was supplied by Hengyuan New Materials Co., Ltd., Huangshan, China, with a density of 2.55 kg/m^3, and its chemical composition is also listed in Table 1. Photographs of raw materials, including cement, RP, GF, and FA, are displayed in Figure 1. Well-graded river sand, with an aggregate size of 0–5 mm and density of 2.61 kg/m^3, satisfied the requirements of Chinese standard GB/T 14684-2022 [43]. A polycarboxylate superplasticizer, complying with Chinese standard JGT 223-2017 [44], was used to control the workability of the mortar.

Table 1. Chemical composition of raw materials.

Material	By Weight/%							
	CaO	SiO_2	Al_2O_3	Fe_2O_3	MgO	SO_3	TiO_2	K_2O
Cement	25.02	55.50	15.42	5.02	1.25	1.01	/	/
FA	3.50	57.03	26.12	4.23	0.72	0.72	1.81	1.34

Table 2. Physical properties of 32.5 cement.

Density/g·cm^{-3}	Setting Time		Flexural Strength		Compressive Strength	
	Initial/min	Final/min	3 d/MPa	28 d/MPa	3 d/MPa	28 d/MPa
3.6	307	373	4.6	6.3	20.6	37.6

Table 3. Physical parameters of glass fiber.

Length/mm	Diameter/μm	Tensile Strength /MPa	Elastic Modulus/GPa	Density/g·cm^{-3}
6	14	1000	72	2.68

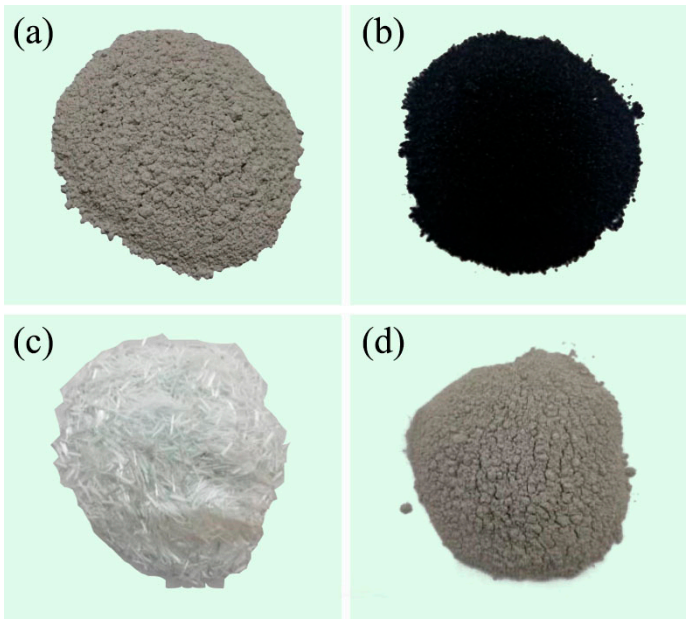

Figure 1. Photographs of raw materials: (**a**) cement; (**b**) RP; (**c**) GF; (**d**) FA.

2.2. Mixed Proportions and Specimens Preparation

In accordance with the proposed scheme outlined in the relevant literature [45,46], we conducted a preliminary experiment to determine the mixed proportions. To evaluate the additives (FA and GF) content on the properties of rubberized mortar, 36 mixes were designed using different volume fractions (0%, 10%, 20%, and 30%) of RP as a partial replacement of fine aggregate. The different dosages of FA (volume fractions of 0%, 5%, and 10% to replace cement) and GF (volume fractions of 0%, 0.2%, and 0.4% with extra incorporation) were also considered. The mixing water/binder and binder/sand weight ratios were set at 1:2 and 2:5, respectively. The dosage of polycarboxylate superplasticizer was kept at 1 wt.%. All the mixed proportions are summarized in Table 4.

Table 4. Design parameter of mixed proportions.

0% RP		10% RP		20% RP		30% RP	
GF/%	FA/%	GF/%	FA/%	GF/%	FA/%	GF/%	FA/%
0	0	0	0	0	0	0	0
0	5	0	5	0	5	0	5
0	10	0	10	0	10	0	10
0.2	0	0.2	0	0.2	0	0.2	0
0.2	5	0.2	5	0.2	5	0.2	5
0.2	10	0.2	10	0.2	10	0.2	10
0.4	0	0.4	0	0.4	0	0.4	0
0.4	5	0.4	5	0.4	5	0.4	5
0.4	10	0.4	10	0.4	10	0.4	10

Note: in FA5GF0.2RP20 specimen, "5", "0.2", and "20" refers to volume fractions of FA, GF, and RP in the mixtures.

To ensure the uniformity of the prepared mortar specimens, the following manufacturing process was adopted to prepare the rubberized mortar modified by FA and GF. Firstly, cement and FA were dry-mixed together in a rotary mixer for 1 min, and then water was added to the mixture and mixed slowly for another 1 min to obtain the mixed slurry. Subsequently, sand, RP, and GF were added in turn to the slurry, and they were stirred at high-speed for 2 min. Finally, after allowing the mortar to stand for 90 s, it was re-stirred at high speed for 1 min, and prepared fresh mortar was obtained. After the completion of the mortar stirring, the freshly prepared mortar specimens were cast in mold and cured for corresponding hydration ages in water with 95 ± 2% relative humidity until testing.

2.3. Fluidity

The fluidity of rubberized mortar was assessed using a mini slump test following the Chinese standard GB/T 2419-2005 [47]. In order to ensure the compactness of mortar, the fresh mortar was poured into the truncated cone model with specific dimensions (height: 60 ± 0.5 mm, upper diameter: 70 ± 0.5 mm, and lower diameter: 100 ± 0.5 mm) and compacted twice by continuous ramming. The diameter of the two vertical directions was measured using a ruler, and the average value was calculated, which represents the fluidity of the mortar.

2.4. Mechanical Properties

Three series of specimens with 40 × 40 × 160 mm size were prepared for each mixed proportions, and these specimens were used to determine their mechanical properties.

The flexural strength and compressive strength were conducted using a compression testing machine (YAW-300C) in accordance with the Chinese standard GB/T 17671-2020 [48]. For the flexural strength test, three specimens with hydration ages of 7 and 28 days were measured when the loading rate was 50 ± 10 N/s. After completing the flexural strength test, a total of six broken specimens were used for the compressive strength test. The loading rate for this test was 2400 ± 200 N/s. The flexural and compressive strength of each specimen were obtained by taking the average value of the test results.

2.5. Drying Shrinkage

According to the Chinese standard JGJ/T 70-2009 [49], the specimen size of the drying shrinkage test is 40 × 40 × 160 mm. The copper shrinkage heads were embedded at both ends of the specimen, and the copper nail was exposed to the end face of the specimen by 8 ± 1 mm, as shown in Figure 2. To ensure accurate shrinkage measurement, the mortar specimens were fully vibrated. Subsequently, the drying shrinkage strain was measured at hydration ages of 14, 28, 56, and 90 days. The value of drying shrinkage (S_i) of each specimen was obtained using Equation (1). To ensure the accuracy of the experimental data, the average value of three specimens was calculated to obtain the drying shrinkage strain.

$$S_i = \frac{L_0 - L_t}{140} \quad (1)$$

where L_0 represents the initial record of the micrometer, L_t represents the record of the micrometer on corresponding days, and 140 is the effective length of the specimens.

Figure 2. Test of the drying shrinkage.

2.6. Impact Resistance

The impact resistance test was conducted using a pendulum with a specified height. The non-notched sample in the cantilever beam state was struck once, and the test equipment is shown in Figure 3. In accordance with the Chinese standard GB/T 1843-2008 [50], the specimens for the impact resistance test had dimensions of 15 × 20 ×160 mm. The pendulum had an impact energy of 11 J, an angle of 50°, and a speed of 2.9 m/s. The results of the impact resistance test were determined using Equation (2):

$$\alpha_i = \frac{W}{h \times b} \tag{2}$$

where α_i is the impact strength of the specimen, W is the absorbing energy as the specimen is destroyed, and h and b represent the thickness and height of the specimen.

Figure 3. Cantilever beam tester.

2.7. Thermal Conductivity

The thermal conductivity of the specimens was measured by a thermal conductivity instrument (CD-DR3030), and this instrument adopts a microcomputer automatic control system, which can automatically control and complete data acquisition, as shown in Figure 4a. In accordance with the Chinese standards GB/T 6342-1996 [51] and GB/T 10294-2008 [52], the specimens, measuring 300 × 300 × 30 mm, were prepared with specific mixed proportions. Prior to the test, the specimens were dried at 105 ± 5 °C until a constant weight was reached to measure their thermal conductivity. The controlling parameters of the thermal conductivity instrument were as follows: the cold and hot plate's temperature

were set at 20 and 40 °C, respectively. Finally, the thermal conductivity values were calculated using Equation (3):

$$\lambda = \frac{wd}{A(T_1 - T_2)} \tag{3}$$

where λ represents thermal conductivity, w is the power of the calorimeter plate, d and A are the average thickness and calculated area of the specimen, and T_1 and T_2 are the cold and hot plate's temperature.

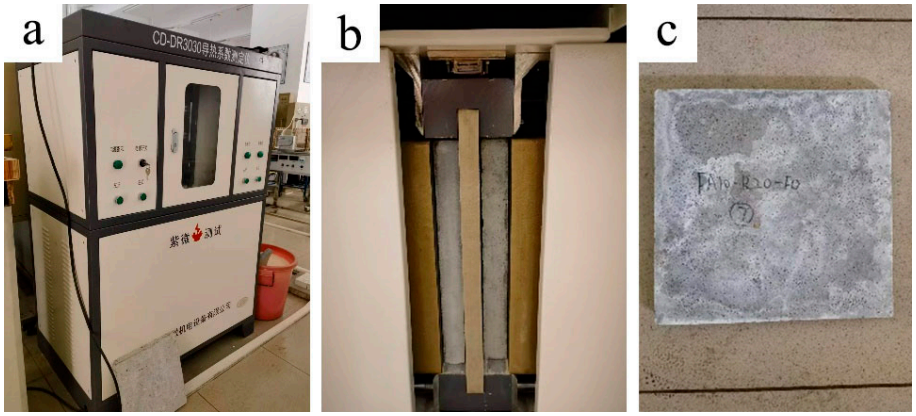

Figure 4. Characterization of thermal conductivity (**a**) measurement instrument; (**b**) thermal insulation test; (**c**) the prepared specimen.

2.8. Microstructure

Scanning electron microscopy (SEM) was conducted to observe the pore structure and interface of rubberized mortar. The specimens were soaked in anhydrous ethanol to terminate hydration and were dried at 60 °C for 2 h for testing. To obtain high-definition SEM images, the specimens were coated with gold to ensure their good electrical conductivity.

2.9. Analytic Hierarchy Process (AHP)

The AHP is a highly effective and commonly used method for analyzing problems related to multi-criterion decision making [53]. The AHP involves breaking down a complex problem into multiple factors and organizing them into a hierarchical structure based on their relationships. The overall ranking of the decision-making scheme is then determined by comparing these factors. The specific implementation process is as follows: (a) The relationship between the various factors in the system was analyzed, and the hierarchical structure of the system was established. (b) Pairwise comparisons were conducted on the nodes at each level, and the results were recorded as a_{ij} (note: i and j represent the relative importance of the node, and the importance values are shown in Table 5). Subsequently, the pairwise comparison matrix was constructed based on Equation (4). (c) Based on the pairwise comparison matrix, the relative weights of each factor were determined using the average values calculated through the arithmetic average method, geometric average method, and eigenvalue method, and the consistency test was performed using Equations (5) and (6). (d) The score was calculated based on the weight matrix, and the levels were ranked to select the best solution.

$$\begin{matrix} \mathrm{A_1}\ \mathrm{A_2} \cdots \mathrm{A_n} \\ \\ \end{matrix} \begin{matrix} \mathrm{A_1} \\ \mathrm{A_2} \\ \vdots \\ \mathrm{A_3} \end{matrix} \begin{bmatrix} a_{1,1} & a_{1,2} & \cdots & a_{1,n} \\ a_{2,1} & a_{2,2} & \cdots & a_{2,n} \\ \vdots & \vdots & & \vdots \\ a_{n,1} & a_{n,2} & \cdots & a_{n,n} \end{bmatrix} \begin{bmatrix} \omega_1 \\ \omega_2 \\ \vdots \\ \omega_\mathrm{n} \end{bmatrix} = n \begin{bmatrix} \omega_1 \\ \omega_2 \\ \vdots \\ \omega_\mathrm{n} \end{bmatrix} \tag{4}$$

$$\mathrm{CI} = \frac{\lambda_{\max} - n}{n - 1} \tag{5}$$

$$CR = \frac{CI}{RI} < 0.1 \quad (6)$$

where A_n is the alternative, ω_n is the associated eigenvector, n is the order of matrix, CI is the consistency index, λ_{max} is the maximum eigen value of the matrix, and RI is the random consistency index.

Table 5. The importance value of step (b) in AHP.

Scales	Importance value of *i* and *j*
1	Equal importance
3	Slightly higher importance
5	Normal importance
7	Strong importance
9	Extreme importance
2, 4, 6, 8	Intermediate value of two adjacent scales

3. Results and Discussions

3.1. Fluidity

Fluidity is an important index reflecting the workability of mortar, which is mainly used to evaluate the flow ability of fresh mortar [54]. Figure 5 demonstrates the impact of varying FA and GF content on the fluidity of rubberized mortar. The figure indicates that the fluidity of fresh rubberized mortars falls within the range of 100–250 mm, satisfying the requirements of the Chinese standard GB/T 2419-2005 [47]. Additionally, the content of FA, GF, and RP has a significant impact on the fluidity of mortar. Consequently, the impact of these additives on fluidity was examined separately, as outlined in the following analysis.

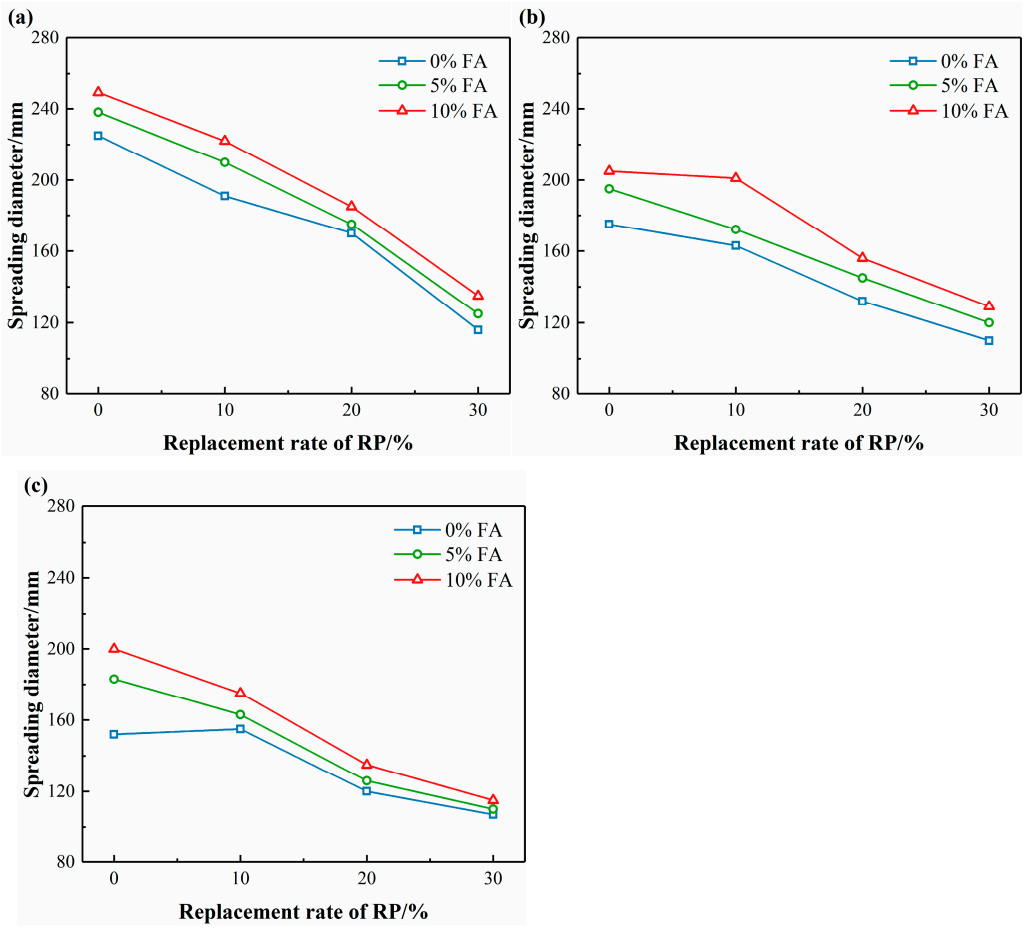

Figure 5. Fluidity of rubberized mortar modified by FA and GF: (**a**) 0% GF; (**b**) 0.2% GF; (**c**) 0.4% GF.

Figure 5a–c represent the change in fluidity of rubberized mortar with different RP contents (0%, 10%, 20%, 30%) under the influence of FA (0%, 5%, 10%) and GF (0%, 0.2%, 0.4%). As we can see from that figure, the addition of RP significantly reduces the fluidity of the mortar. In the specimens with only RP mixed, the fluidity of the mortar decreases from 225 mm to 116 mm as the RP content increases from 0% to 30%. This decrease in fluidity can be attributed to the high water absorption capacity of RP and its rough jagged-like edges. Similar findings have been reported in studies conducted by Abd-Elaty et al., Mostofinejad et al., and Zhai et al. [20,22,55]. The addition of GF also leads to a decrease in fluidity, as the surface of GF has a strong friction with paste, increasing the viscosity of the mixture [56]. Besides that, the increase in the GF dosage may increase the risk of agglomeration. However, the addition of FA improves the fluidity of mortar, particularly at higher levels of FA substitution. This is attributed to the smooth surface morphology of FA, which promotes a good "ball-bearing effect" on the contact surface between aggregate and paste [29,57]. Similar observations were observed in the research conducted by Shao et al. [30,32]. The fluidity of the rubberized mortar under the joint action of FA and GF has been altered to some extent. The addition of GF and RP to the mortar leads to a significant decrease in fluidity. For instance, the fluidity of the specimens with only 0.4% GF, increasing the percentage of RP from 0% to 20%, caused an increase in the fluidity value by 32 mm (21%). However, FA can effectively mitigate the negative impact of the decreased fluidity caused by GF and RP. For the specimens with 0.4% GF and 20% RP, increasing the percentage of FA from 0% to 10% caused an increase in the fluidity value by 15 mm (12%). This result indicates that increasing the amount of FA appropriately has a more pronounced effect on improving the fluidity of rubberized mortar modified by GF.

3.2. Mechanical Properties

3.2.1. Flexural Strength

Figure 6a–c present the results of the flexural strength test for rubberized mortar modified by FA and GF at 7 and 28 days. At 7 days, the flexural strength decreased as the RP replacement rate increased, although the decrease was somewhat mitigated. This decrease can be attributed to the inadequate adhesion between the RP and cement matrix, as well as the impact of RP as an aggregate on the overall stiffness. The flexural strength of rubberized mortar has almost been improved by the influence of GF. Only the flexural strength of specimen FA0GF0.2RP20 (3.7 MPa) did not show an improvement compared to specimen FA0GF0RP20 (3.7 MPa). This could be attributed to the incomplete bonding between GF and mortar at 7 days, as well as the relatively small GF content. Moreover, the flexural strength exhibited a more significant increase when the GF content reached 0.4%. The experimental data also indicated a similar change rule after the addition of FA. However, the overall flexural strength was slightly reduced due to the low early hydration activity of FA and its dilution effect [58,59].

At 28 days, the addition of RP resulted in a decrease in flexural strength. When the specimens were mixed with only RP, with replacement rates of 10%, 20%, and 30%, the flexural strength decreased by 22.7%, 41.8%, and 57.3%, respectively. This decline is higher compared to that at 7 days. Additionally, the inclusion of GF enhances the 28-day flexural strength of rubberized mortar, with a more pronounced effect observed in rubberized mortar with a higher RP replacement rate. For instance, the flexural strength of specimens with only 30% RP, increasing the dosage of GF from 0% to 0.2% and 0.4%, caused an increase in the flexural strength value by 0.7 MPa (14.9%) and 1.3 MPa (29.8%), respectively. This phenomenon can still be observed even after incorporating the FA additive, with an increase of 14.3% and 22.4% (with 5% FA) and 14.3 and 28.6% (with 10% FA), respectively.

We recorded the failure modes of the two specimens with specific mixed proportions and observed their crack development during the experimental process. The failure mode of pure cement mortar is shown in Figure 7a, where obvious brittle failure characteristics were observed during the failure process, and the specimen was disconnected from the middle of the specimen. On the other hand, Figure 7b illustrates the failure mode of

rubberized mortar modified by GF. It can be observed that there were no obvious cracks, and crack development did not occur in the middle of the specimen, indicating typical ductile failure characteristics. Similar phenomena and conclusions have also been reported by Ma et al., Li et al., and Xu et al. [1,2,60].

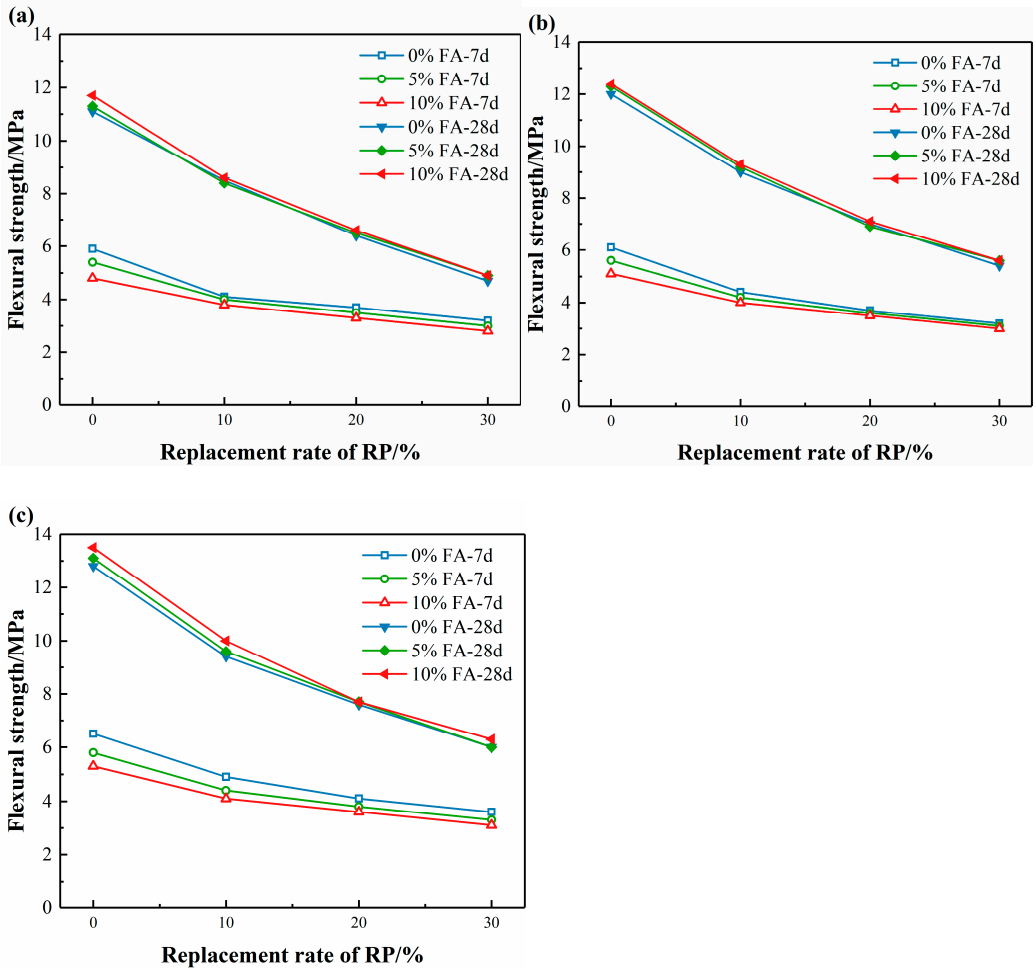

Figure 6. Flexural strength of rubberized mortar modified by FA and GF: (**a**) 0% GF; (**b**) 0.2% GF; (**c**) 0.4% GF.

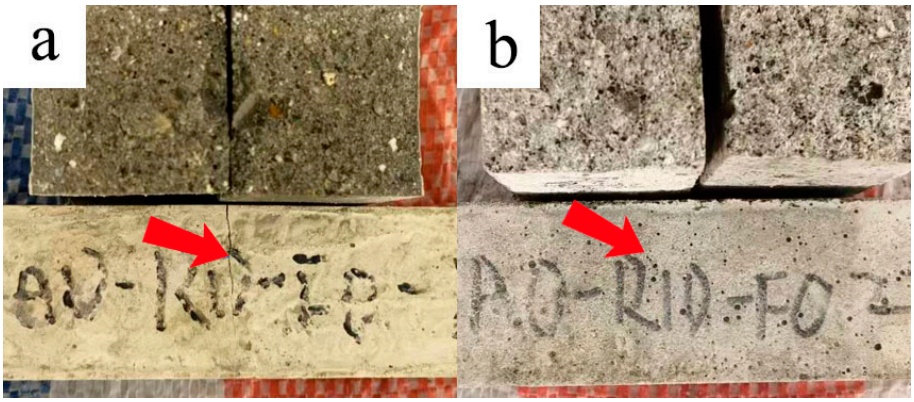

Figure 7. Failure mode of mortar: (**a**) FA0GF0RP0; (**b**) FA0GF0.2RP10.

3.2.2. Compressive Strength

The compressive strength trend of rubberized mortar modified by FA and GF is similar to the flexural strength, which is shown in Figure 8. At 7 days, when the replacement rate of RP to replace sand in the mixture increased from 0% to 30%, the compressive strength exhibited varying degrees of decline. Specifically, the rubberized mortar specimens with RP replacement rates of 10%, 20%, and 30% experienced an average reduction in compressive strength of 37.0%, 49.0%, and 65.6%, respectively, compared to the pure cement specimen. The incorporation of GF did not significantly improve the compressive strength of the sample compared to its effect on the flexural strength. In fact, in some specimens (FA5GF0.2R20 and FA5GF0.2R30), there was a decrease in compressive strength. This observation could be attributed to the relatively short curing time and the weak bonding between the fiber and the matrix. The incorporation of FA typically led to a decrease in the 7-day compressive strength of mortar. However, exceptions can be observed in certain specimens with a high RP content (FA5GF0R20 and FA5GF0R30), where a slight improvement of 4.0% and 5.9% is observed compared to the pure cement specimen. Based on these experimental findings, it can be inferred that there is a certain synergistic effect between FA and RP in enhancing compressive strength.

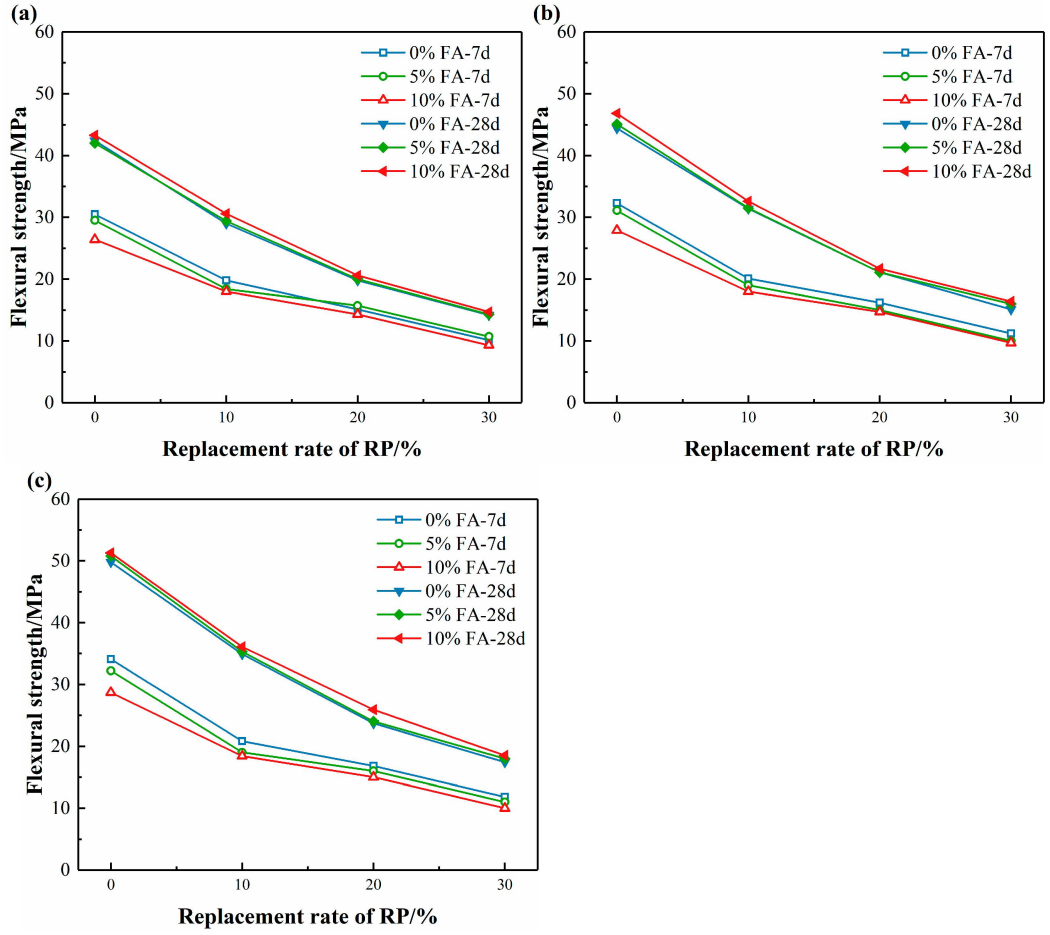

Figure 8. Compressive strength of rubberized mortar modified by FA and GF: (**a**) 0% GF; (**b**) 0.2% GF; (**c**) 0.4% GF.

At 28 days, the addition of RP also resulted in a decrease in compressive strength. When the RP replacement rate to replace sand in the mixture was 10%, 20%, and 30%, the compressive strength of the rubberized mortar was 31.6%, 53.3%, and 66.5% lower than that of the pure cement group, respectively. The decline in compressive strength gradually decreases as the RP replacement rate increases. In contrast to the 7-day results, GF has a significant positive effect on the 28-day compressive strength of mortar, and this effect becomes more pronounced with higher RP replacement rates. The addition of 0.2% GF and 10% RP to the specimens resulted in a slight increase in the 28-day compressive strength value. When the dosage of FA was increased from 0% to 5% and 10%, the 28-day compressive strength value increased by 8.3%, 7.1%, and 6.5%, respectively, compared to specimens without GF. Similarly, when the GF dosage increased to 0.4%, this ratio became 20.3%, 20.1%, and 18.0%. Additionally, the addition of 0.2% GF and 20% RP to the specimens also led to an improvement in the 28-day compressive strength. Specifically, when the dosage of FA increased from 0% to 5% and 10%, the 28-day compressive strength value increased by 6.6%, 5.5%, and 5.3%, respectively, compared to the specimens without GF. When the dosage of GF increased to 0.4%, the improvement rates changed to 19.7%, 20.0%, and 25.7%. These findings suggest that the addition of GF can effectively enhance the 28-day compressive strength of rubberized mortar, while the impact of FA is not significant.

In a previous study, Zhao et al. [31] discovered that FA decreased the strength of the rubber–cement matrix, consequently impacting the compressive strength. However, this phenomenon was not prominently observed in this study. Additionally, Li et al. and Qaidi et al. [61,62] suggested that the improved compressive strength resulting from the presence of fibers is primarily attributed to their ability to restrict crack development and provide lateral restraint. These findings align with the conclusions drawn in this study.

3.3. Drying Shrinkage

Drying shrinkage is an important phenomenon that assesses the deformation behavior in cementitious materials, which is closely related to their structural and durability properties [63]. Moreover, according to the relevant literature [64], drying shrinkage is directly influenced by the amount of free water in the system and the porosity of the cementitious materials.

Figure 9 displays the results of the drying shrinkage test for rubberized mortar modified by FA and GF at various hydration ages. As the hydration age increases, the drying shrinkage value consistently rises. However, the slope of the drying shrinkage curve for nearly all specimens noticeably decreases after 28 days. This can be attributed to the fact that the hydration process within the mortar is essentially finished within 28 days, causing the growth rate of dry shrinkage to decelerate.

The addition of RP has a varying effect on the drying shrinkage of mortar. When the RP replacement rate is low ($\leq$ 10%), as shown in Figure 9a,b, the dry shrinkage value of the mortar does not change significantly. The 28-day drying shrinkage values of specimens FA0GF0RP0 and FA0GF0RP10 were 442.9 and 450.0 με, respectively. When the RP replacement rate is large ($\geq$ 20%), the 28-day drying shrinkage has a significant increase, with specimen FA0GF0RP30 reaching 700.0 με. These phenomena may be mainly related to the porous structure of RP particles and high water absorption capacity. Under the condition of a large replacement rate, it is easy to cause the rapid growth of the dry shrinkage value of mortar. Similar conclusions have been drawn in the research conducted by Uygunoğlu et al. and Su et al. [65,66]. Additionally, Deng et al. [67] reported that the soft nature (high elasticity) characteristic of RP resulted in it being more prone to deformation behavior, which reduced the resistance to the drying shrinkage-induced strain of the matrix.

The addition of GF can effectively reduce the drying shrinkage of rubberized mortar at varying hydration ages. Especially, the drying shrinkage first decreased as the GF content increased to 0.2%, followed by a certain decrease as it further increased to 0.4%. However, this decrease is more significant when the RP replacement rate is higher ($\geq$20%), as displayed in Figure 9c,d. The main reason for this is that the binding force provided

by GF effectively limits the deformation of the matrix during the evaporation of water, and the specimens with a larger RP replacement rate need more GF to provide sufficient stiffness for the matrix. In the study conducted by Chen et al. [68], they found that the addition of excessive fiber may enhance the pore connectivity inside the matrix, which has a negative impact on the drying shrinkage of the matrix. Consequently, this should be fully considered in the design of this type of material.

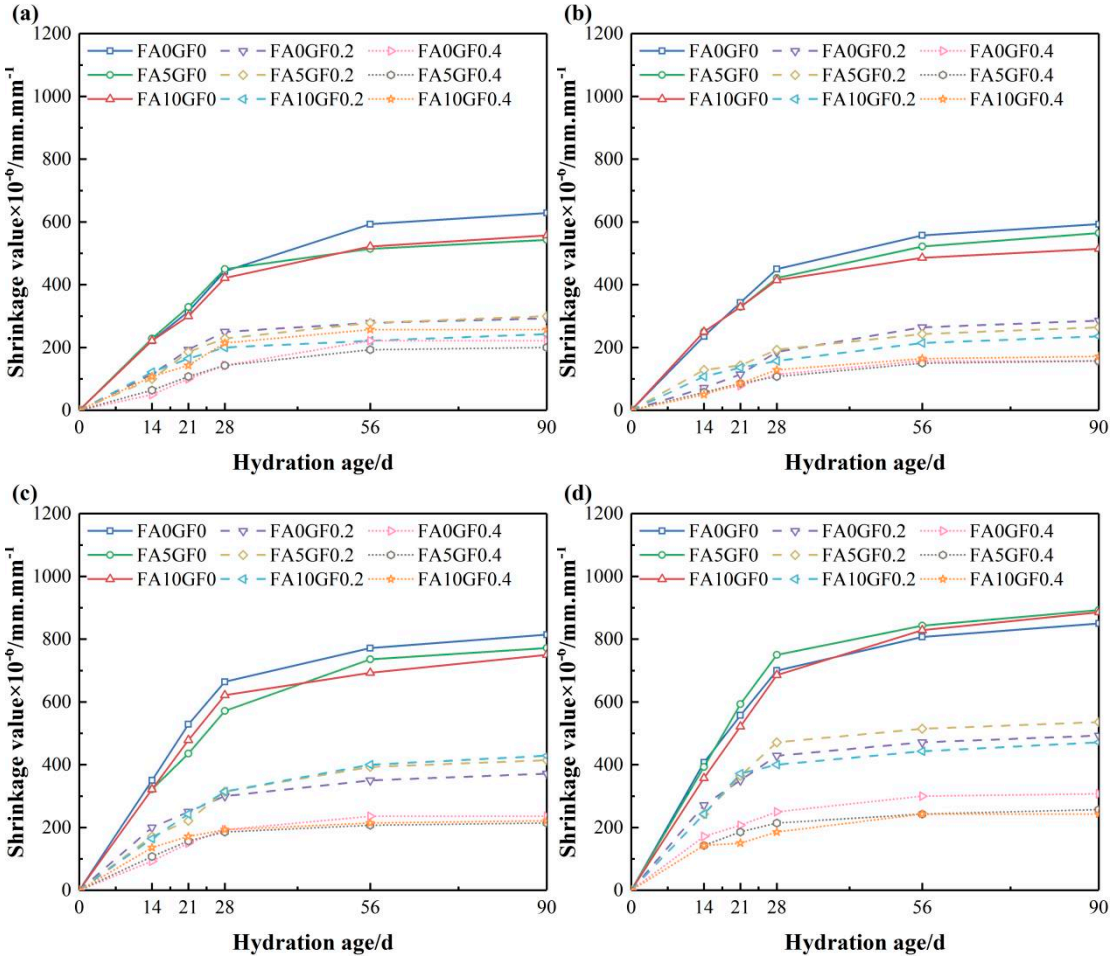

Figure 9. Drying shrinkage of rubberized mortar modified by FA and GF: (**a**) 0% RP; (**b**) 10% RP; (**c**) 20% RP; (**d**) 30% RP.

The effect of FA on the drying shrinkage of rubberized mortar is less than that of RP and GF. During the 28-day hydration age, the addition of FA generally reduces the drying shrinkage of rubberized mortar. However, after the hydration age exceeds 28 days, the specimens modified by FA generally have relatively high drying shrinkage values. In the relevant literature [69–71], the reasons for this phenomenon are summarized as follows: (1) The early hydration activity of FA is relatively low, resulting in low drying shrinkage in early hydration ages. (2) FA changes the original composition of the cementitious materials system, which in turn changes the overall pore structure. (3) The addition of FA effects the carbon resistance ability of the cement matrix; this may affect the porosity of the cementitious materials system.

3.4. Impact Resistance

Impact resistance is an important factor in evaluating toughness. Figure 10 presents the results of the impact resistance test conducted on rubberized mortar modified by FA and GF. It can be seen from the figure that when the RP replacement rate is below 20%, the impact resistance of the mortar only shows a slight improvement. When the RP replacement rate reaches 30% (as shown in Figure 10d), there is a significant enhancement in the impact resistance of the mortar. This enhancement can be attributed to the unique physical properties of RP, which enable the formation of elastic centers within the concrete and contribute to the improved toughness of the mortar. This observation aligns with previous research findings [72,73]. The addition of GF has a significant impact on improving the impact resistance of rubberized mortar. As the dosage of GF increases from 0% to 0.4%, the impact resistance of each mixture in the test group can be increased by 26–35%. This increase in impact resistance is due to the enhancement of mortar toughness, which helps to restrict the development of cracks in the mortar under impact load. It is worth noting that the FA content does not have a significant effect on the impact resistance of rubberized mortar.

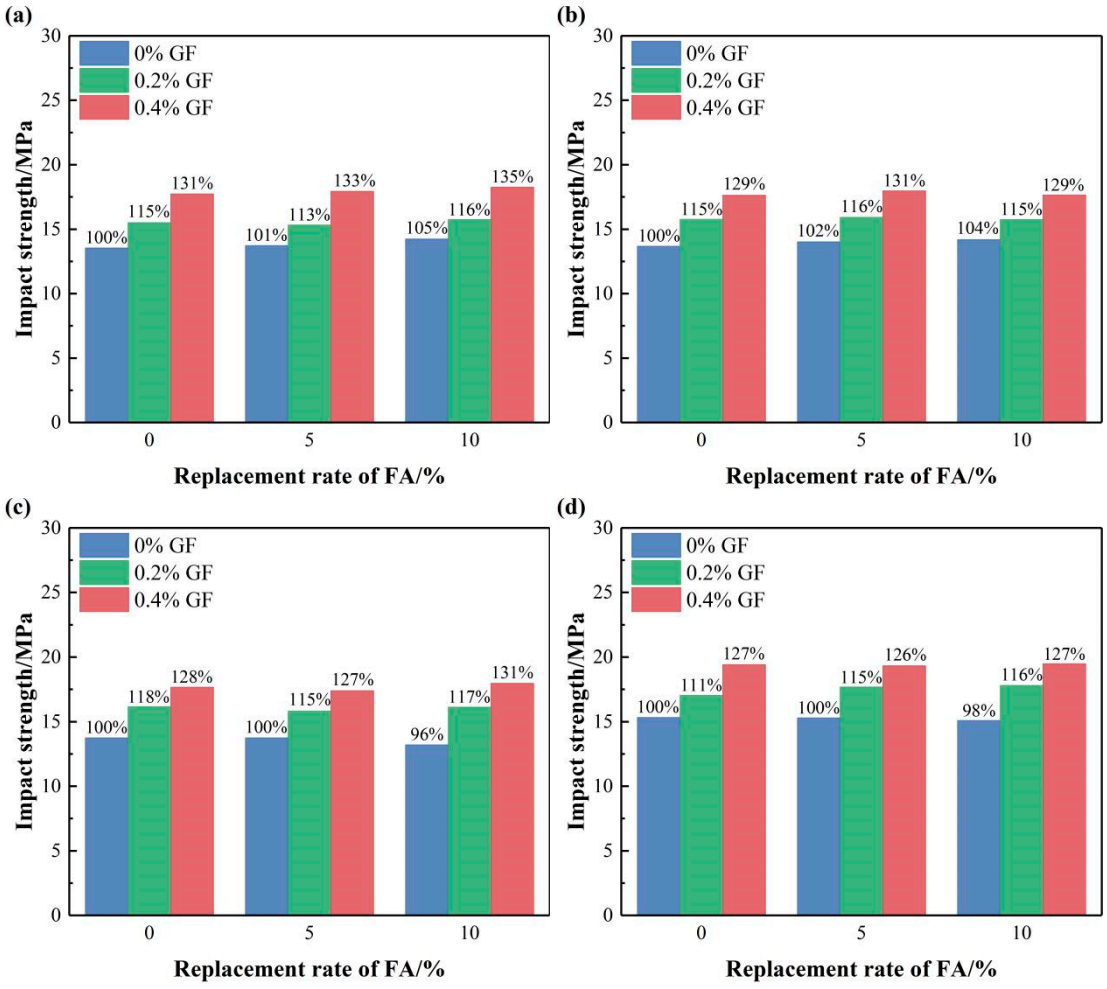

Figure 10. Impact strength of rubberized mortar modified by FA and GF: (**a**) 0% RP; (**b**) 10% RP; (**c**) 20% RP; (**d**) 30% RP.

3.5. Thermal Insulation Properties

Based on the results of the varying properties test of rubberized mortar modified by FA and GF on the above sections, it was observed that a dosage of 10% FA can enhance the workability of the mortar while preserving its mechanical and deformation resistance properties. To streamline the experimental process, we conducted the following experiments

using a 10% FA dosage. Additionally, we performed a thermal conductivity test based on the mix formulation provided in Table 4.

Thermal conductivity is an important parameter for the evaluation of insulating material [74]. The lower the thermal conductivity, the better the thermal insulating properties of the material, that is, the increase in the internal insulation quality of the content. Figure 11 illustrates the thermal conductivity of rubberized mortar specimens. The figure shows that the addition of RP significantly reduces the thermal conductivity of the mortar. As the RP replacement rate increases from 0% to 30%, thermal conductivity decreases from approximately 0.36–0.39 $W \cdot (m \cdot K)^{-1}$ to 0.23–0.25 $W \cdot (m \cdot K)^{-1}$. This enhancement in the thermal insulation properties can be attributed to the relatively low density of RP and its lower thermal conductivity compared to sand. Similar findings were reported in a study conducted by Abd-Elaty et al. [55]. Furthermore, the addition of GF also enhances the thermal insulation properties of rubberized mortar, albeit to a lesser extent. This can be attributed to the thermal physical properties of GF and its impact on the internal pore structure of mortar. However, the relatively small quantity of GF present in rubberized mortar limits the extent of this improvement. These results corroborate the findings of Awoyera et al. and Guardia et al. [75,76], identifying improved thermal insulating properties with increased fiber materials.

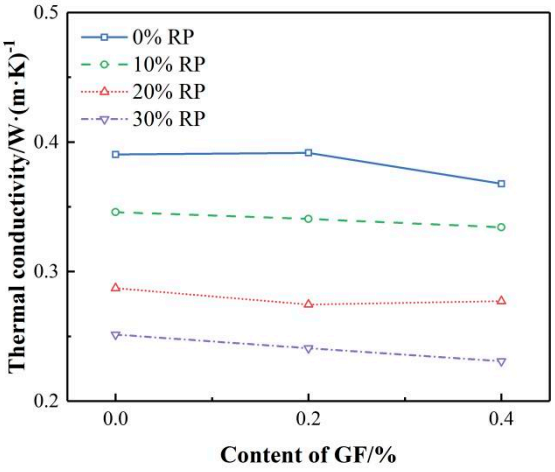

Figure 11. Thermal conductivity of rubberized mortar.

The utilization of waste materials for the production of building insulation materials can enhance thermal comfort in buildings while also offering cost-effective construction and environmental advantages. The aforementioned experimental results provide valuable insights into the potential applications of waste rubber and GF in various thermal insulation requirements.

3.6. Microstructure

Figure 12 illustrates the morphologies of rubberized mortar. In Figure 12a,b, voids and cracks can be observed around RP, suggesting that the damage in the rubberized mortar primarily occurs between the RP and matrix. These observations are consistent with previous studies [12,16,59]. However, the friction in cracks may result in energy dissipation. In Figure 12c,d, it is evident that the number of cracks in rubberized mortar is significantly reduced after the addition of GF. This improved interface has a positive impact on the strength and toughness of rubberized mortar. Although micro pores are present in rubberized mortar containing GF, the enhanced thermal insulation properties (in Section 3.5) may relate to this special observation.

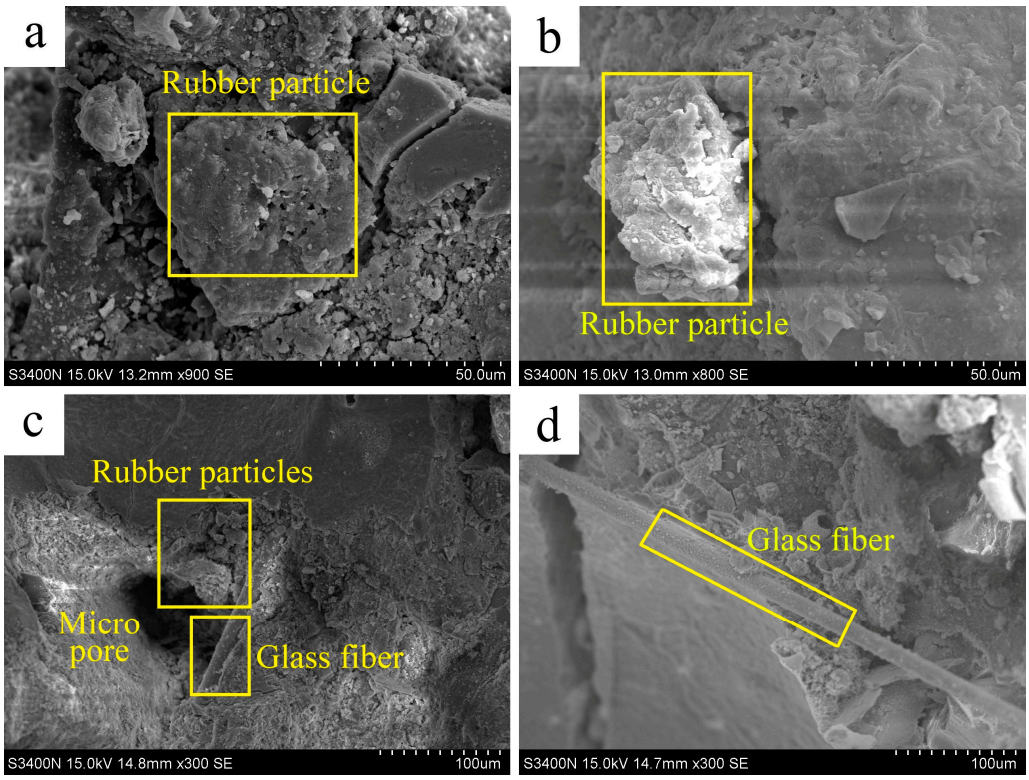

Figure 12. Microstructure: (**a**,**b**) are rubberized mortar; (**c**,**d**) are rubberized mortar containing GF.

3.7. Analytical Hierarchy Process

In this section, the AHP method was adopted to determine the optimal mixed proportion of rubberized mortar modified by FA and GF. The criteria considered were fluidity (C1), flexural strength (C2), compressive strength (C3), impact strength (C4), drying shrinkage (C5), and thermal conductivity (C6). Based on the comprehensive analysis of FA, GF, and RP on the properties of mortar in this study, six specimens (FA10GF0.2RP10, FA10GF0.4RP10, FA10GF0.2RP20, FA10GF0.4RP20, FA10GF0.2RP30, and FA10GF0.4RP30) were selected as alternatives, as shown in Figure 13.

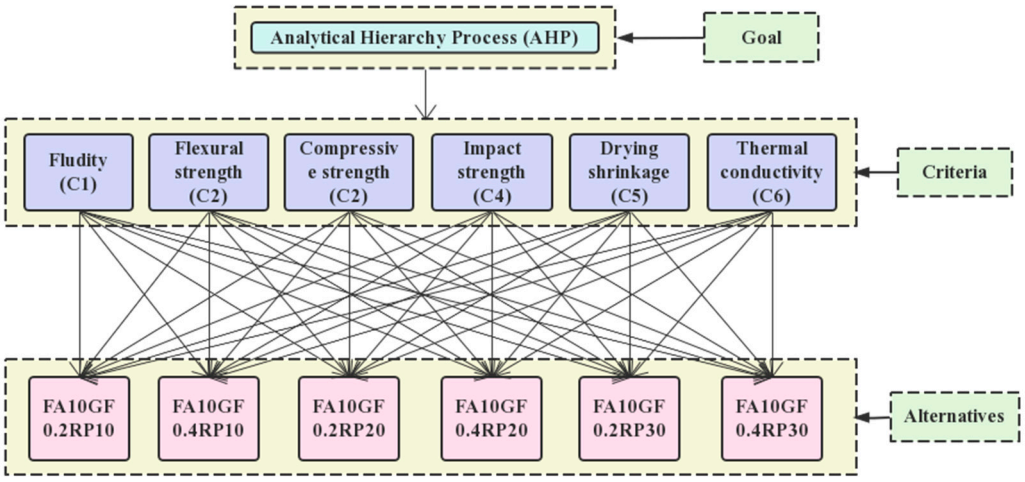

Figure 13. Flow chart of the AHP.

According to the step described in Table 5, the order of six property indicators (C1, C2, . . ., C6) is sorted. Then, the pairwise comparisons matrix G was constructed as below:

$$G = \begin{bmatrix} 1 & 1/3 & 1/3 & 5 & 3 & 1/3 \\ 3 & 1 & 1 & 7 & 5 & 1 \\ 3 & 1 & 1 & 7 & 5 & 1 \\ 1/5 & 1/7 & 1/7 & 1 & 1/2 & 1/7 \\ 1/3 & 1/5 & 1/5 & 2 & 1 & 1/5 \\ 3 & 1 & 1 & 7 & 5 & 1 \end{bmatrix}$$

After calculating, the maximum eigen (λ_{max}) of the pairwise comparisons matrix G and its corresponding eigenvector (v) were obtained as shown below:

$$\lambda_{max} = 6.0898$$

$$v = (0.2380, 0.5560, 0.5560, 0.0667, 0.1073, 0.5560)^T$$

The consistency test was performed using Equations (5) and (6), as the following equation:

$$\text{CI} = \frac{\lambda_{max} - n}{n-1} = 0.01796$$

$$\text{CR} = \frac{\text{CI}}{\text{RI}} = 0.0145 < 0.1$$

After satisfying the consistency test, the arithmetic average method, geometric average method, and eigenvalue method were used to calculate the weight (ω_1, ω_2, and ω_3), and their average values were calculated as the final weight vector (ω_G), as shown below:

$$\begin{aligned} \omega_1 &= (0.1155 \quad 0.2664 \quad 0.2664 \quad 0.0326 \quad 0.0525 \quad 0.2664)^T \\ \omega_2 &= (0.1111 \quad 0.2661 \quad 0.2661 \quad 0.0316 \quad 0.0512 \quad 0.2661)^T \\ \omega_3 &= (0.1144 \quad 0.2673 \quad 0.2673 \quad 0.0321 \quad 0.0516 \quad 0.2673)^T \\ \omega_G &= (0.1137 \quad 0.2666 \quad 0.2666 \quad 0.0321 \quad 0.0518 \quad 0.2666)^T \end{aligned}$$

Based on the final weight calculation result, the priority of the six properties indicators can be determined. In order to consider the quantitative differences in their importance, pairwise comparison matrices are provided for each indicator, denoted as C1, C2, . . ., C6:

$$\text{C1} = \begin{bmatrix} 1 & 2 & 3 & 4 & 5 & 6 \\ 1/2 & 1 & 2 & 3 & 4 & 5 \\ 1/3 & 1/2 & 1 & 2 & 3 & 4 \\ 1/4 & 1/3 & 1/2 & 1 & 2 & 3 \\ 1/5 & 1/4 & 1/3 & 1/2 & 1 & 2 \\ 1/6 & 1/5 & 1/4 & 1/3 & 1/2 & 1 \end{bmatrix} \text{C2} = \begin{bmatrix} 1 & 1/2 & 5 & 4 & 8 & 7 \\ 2 & 1 & 6 & 5 & 9 & 8 \\ 1/5 & 1/6 & 1 & 1/2 & 3 & 2 \\ 1/4 & 1/5 & 2 & 1 & 4 & 3 \\ 1/8 & 1/9 & 1/3 & 1/4 & 1 & 1/2 \\ 1/7 & 1/8 & 1/2 & 1/3 & 2 & 1 \end{bmatrix}$$

$$\text{C3} = \begin{bmatrix} 1 & 1/2 & 6 & 5 & 8 & 7 \\ 2 & 1 & 7 & 6 & 9 & 8 \\ 1/6 & 1/7 & 1 & 1/2 & 3 & 2 \\ 1/5 & 1/6 & 2 & 1 & 4 & 3 \\ 1/8 & 1/9 & 1/3 & 1/4 & 1 & 1/2 \\ 1/7 & 1/8 & 1/2 & 1/3 & 2 & 1 \end{bmatrix}$$

$$\text{C4} = \begin{bmatrix} 1 & 1/4 & 1/2 & 1/5 & 1/4 & 1/7 \\ 4 & 1 & 2 & 1/2 & 1 & 1/4 \\ 2 & 1/2 & 1 & 1/3 & 1/2 & 1/5 \\ 5 & 2 & 3 & 1 & 2 & 1/3 \\ 4 & 1 & 2 & 1/2 & 1 & 1/4 \\ 7 & 4 & 5 & 3 & 4 & 1 \end{bmatrix}$$

$$\text{C5} = \begin{bmatrix} 1 & 3 & 1/4 & 1 & 1/5 & 1 \\ 1/3 & 1 & 1/6 & 1/3 & 1/7 & 1/3 \\ 4 & 6 & 1 & 4 & 1/2 & 4 \\ 1 & 3 & 1/4 & 1 & 1/5 & 1 \\ 5 & 7 & 2 & 5 & 1 & 5 \\ 1 & 3 & 1/4 & 1 & 1/5 & 1 \end{bmatrix} \text{C6} = \begin{bmatrix} 1 & 1/2 & 1/3 & 1/4 & 1/5 & 1/6 \\ 2 & 1 & 1/2 & 1/3 & 1/4 & 1/5 \\ 3 & 2 & 1 & 1/2 & 1/3 & 1/4 \\ 4 & 3 & 2 & 1 & 1/2 & 1/3 \\ 5 & 4 & 3 & 2 & 1 & 1/2 \\ 6 & 5 & 4 & 3 & 2 & 1 \end{bmatrix}$$

After calculating, their λ_{max}, CI, and CR value are displayed in Table 6. These calculation results can meet the requirements of the consistency test. Then, their weight vector (ω) was obtained as shown below:

$$\omega_{C1} = (0.3825 \quad 0.2504 \quad 0.1596 \quad 0.1006 \quad 0.0641 \quad 0.0428)^T$$

$$\omega_{C2} = (0.3071 \quad 0.4342 \quad 0.0722 \quad 0.1101 \quad 0.0312 \quad 0.0452)^T$$

$$\omega_{C3} = (0.3179 \quad 0.4430 \quad 0.0658 \quad 0.0996 \quad 0.0302 \quad 0.0435)^T$$

$$\omega_{C4} = (0.0393 \quad 0.1240 \quad 0.0702 \quad 0.2053 \quad 0.1240 \quad 0.4372)^T$$

$$\omega_{C5} = (0.0862 \quad 0.0378 \quad 0.2871 \quad 0.0862 \quad 0.4166 \quad 0.0862)^T$$

$$\omega_{C6} = (0.0416 \quad 0.0619 \quad 0.0969 \quad 0.1532 \quad 0.2401 \quad 0.4064)^T$$

Table 6. The maximum eigen, CI, and CR values of pairwise comparison matrices.

Alternatives	C1	C2	C3	C4	C5	C6
λ_{max}	6.1225	6.1605	6.2224	6.1081	6.1168	6.2306
CI	0.0245	0.0321	0.0440	0.0216	0.0234	0.0461
CR	0.0198	0.0259	0.0359	0.0174	0.0188	0.0372

Accordingly, the calculated priorities of alternatives with respect to the overall service performances of rubberized mortar modified by FA and GF are displayed in Figure 14. A higher priority indicates better overall properties. Consequently, the order of priority is as follows: C2 > C1 > C6 > C3 > C5 > C4. Overall, specimen FA10GF0.4RP10 has the highest priority of 0.381.

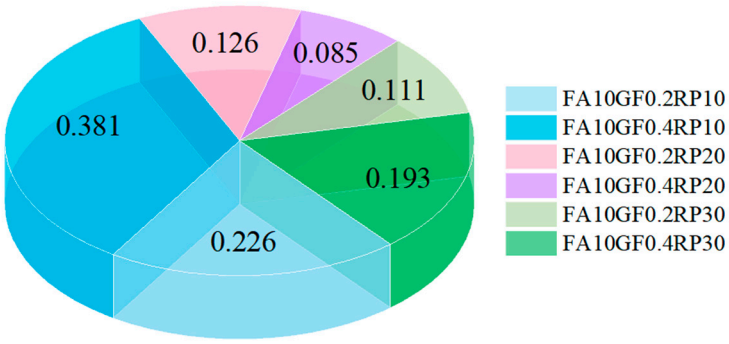

Figure 14. Priorities of rubberized mortar modified by FA and GF.

4. Conclusions

This study aimed to assess the feasibility of incorporating additives (FA and GF) into rubberized mortar. The experiment evaluated the resulting mortars based on fluidity, mechanical properties, drying shrinkage, impact resistance, and thermal insulation properties. The main findings can be drawn as follows:

1. The replacement of RP in mortar leads to a significant decrease in fluidity, and the addition of GF also contributes to reduced fluidity. Moreover, the addition of FA can appropriately improve the fluidity of the mortar. However, achieving this significant reduction in fluidity loss may necessitate the utilization of additional methods, such as incorporating chemical additives.
2. The addition of RP results in a decrease in compressive and flexural strengths. GF has a positive impact on the mechanical properties of rubberized mortar, particularly in enhancing flexural strength. Furthermore, the influence of FA on the mechanical properties of rubberized mortar is not clearly evident.

3. The high replacement rate of RP in the mortar results in a significant increase in drying shrinkage. GF limits the deformation of the matrix during the internal water evaporation process and enhances stiffness, thereby effectively reducing the drying shrinkage of the rubberized mortar. FA initially reduces drying shrinkage within 28 days, but it subsequently leads to an increase in drying shrinkage after 28 days.
4. The addition of RP to mortar can increase its toughness, resulting in improved impact resistance of the specimens. The highest increase in impact resistance is observed when the replacement rate of RP is 30%. GF can effectively restrict the development of cracks in rubberized mortar when subjected to impact loads, while FA has a lesser effect on modifying the impact resistance of rubberized mortar.
5. The low density and low thermal conductivity of RP contribute to the reduction in thermal conductivity of rubber mortar. As the RP replacement rate increases from 0% to 30%, the thermal conductivity decreases to 0.23–0.25 $W \cdot (m \cdot K)^{-1}$. The addition of GF can further decrease the thermal conductivity of rubberized mortar.
6. In the condition of emphasizing fluidity, mechanical properties, drying shrinkage, impact resistance, and thermal insulation properties, the AHP method suggests that specimen FA10GF0.4RP10 exhibits the best comprehensive properties, with the highest priority of 0.381. The AHP method is primarily employed to identify viable options using existing indicators. To expand the applicability of this analytical tool, it may be necessary to foster creativity.

Author Contributions: Conceptualization, F.L.; methodology, Y.Z.; formal analysis, H.L. and Z.L.; data curation, Z.P., H.Z. and X.L.; writing—original draft preparation, H.L.; writing—review and editing, Z.P.; visualization, D.W.; supervision, F.L.; project administration, D.W.; funding acquisition, X.L. All authors have read and agreed to the published version of the manuscript.

Funding: This research was funded by [the National Natural Science Foundation of China] grant number [12072080] and [the Natural Science Foundation of Fujian Province] grant number [2023J011044].

Data Availability Statement: Date will be available on request.

Acknowledgments: The authors gratefully acknowledge the financial support provided by the National Natural Science Foundation of China under Grant No. 12072080 and the Natural Science Foundation of Fujian Province under Grant No. 2023J011044 (in China).

Conflicts of Interest: The authors declare that there is no conflict of interest.

References

1. Xu, J.; Houndehou, J.D.; Wang, Z.; Ma, Q. Experimental investigation on the mechanical properties and damage evolution of steel-fiber-reinforced crumb rubber concrete with porcelain tile waste. *Constr. Build. Mater.* **2023**, *370*, 130643. [CrossRef]
2. Chen, Z.; Li, L.; Xiong, Z. Investigation on the interfacial behaviour between the rubber-cement matrix of the rubberized concrete. *J. Clean. Prod.* **2019**, *209*, 1354–1364. [CrossRef]
3. Abdelmonem, A.; El-Feky, M.S.; Nasr, E.-S.A.R.; Kohail, M. Performance of high strength concrete containing recycled rubber. *Constr. Build. Mater.* **2019**, *227*, 116660. [CrossRef]
4. Roychand, R.; Gravina, R.J.; Zhuge, Y.; Ma, X.; Youssf, O.; Mills, J.E. A comprehensive review on the mechanical properties of waste tire rubber concrete. *Constr. Build. Mater.* **2020**, *237*, 117651. [CrossRef]
5. Raffoul, S.; Garcia, R.; Pilakoutas, K.; Guadagnini, M.; Medina, N.F. Optimisation of rubberised concrete with high rubber content: An experimental investigation. *Constr. Build. Mater.* **2016**, *124*, 391–404. [CrossRef]
6. Youssf, O.; Hassanli, R.; Mills, J.E. Mechanical performance of FRP-confined and unconfined crumb rubber concrete containing high rubber content. *J. Build. Eng.* **2017**, *11*, 115–126. [CrossRef]
7. Ji, Y.; Sun, Q. Experimental and numerical investigation of recycled rubber foam concrete. *Alex. Eng. J.* **2023**, *76*, 573–594. [CrossRef]
8. Assaggaf, R.A.; Ali, M.R.; Al-Dulaijan, S.U.; Maslehuddin, M. Properties of concrete with untreated and treated crumb rubber—A review. *J. Mater. Res. Technol.* **2021**, *11*, 1753–1798. [CrossRef]
9. Xiong, Z.; Fang, Z.; Feng, W.; Liu, F.; Yang, F.; Li, L. Review of dynamic behaviour of rubberised concrete at material and member levels. *J. Build. Eng.* **2021**, *38*, 102237. [CrossRef]
10. Etli, S. Evaluation of the effect of silica fume on the fresh, mechanical and durability properties of self-compacting concrete produced by using waste rubber as fine aggregate. *J. Clean. Prod.* **2023**, *384*, 135590. [CrossRef]

11. Letelier, V.; Bustamante, M.; Olave, B.; Martínez, C.; Ortega, J.M. Properties of mortars containing crumb rubber and glass powder. *Dev. Built Environ.* **2023**, *14*, 100131. [CrossRef]
12. He, S.; Li, L.; Xiong, Z.; Zhang, H.; Zheng, J.; Su, Y.; Liu, F. Effects of ring-type and straight steel fibres on the compressive performance of rubber-recycled aggregate concrete. *J. Build. Eng.* **2023**, *76*, 107148. [CrossRef]
13. Agrawal, D.; Waghe, U.; Ansari, K.; Dighade, R.; Amran, M.; Qader, D.N.; Fediuk, R. Experimental effect of pre-treatment of rubber fibers on mechanical properties of rubberized concrete. *J. Mater. Res. Technol.* **2023**, *23*, 791–807. [CrossRef]
14. Li, H.; Li, Y.; Xiong, Z.; Shu, Z.; Hong, Y.; Chen, S.; Su, Y. Experimental and theoretical study on elliptical rubber concrete filled double-skin GFRP short tubes under axial compression. *Constr. Build. Mater.* **2023**, *401*, 132796. [CrossRef]
15. Zhen, H.; Xiong, Z.; Song, Y.; Li, L.; Qiu, Y.; Zou, X.; Chen, B.; Chen, D.; Liu, F.; Ji, Y. Early mechanical performance of glass fibre-reinforced manufactured sand concrete. *J. Build. Eng.* **2024**, *83*, 108440. [CrossRef]
16. Li, X.; Zhao, Y.; Yao, W.; Wu, B.; Xia, K. Dynamic fracture behaviors of rubberized mortars with various rubber powder sizes and volume percentages. *Eng. Fract. Mech.* **2022**, *269*, 108553. [CrossRef]
17. Yu, F.; Chen, Y.; Fang, Y.; Xu, P.; Xu, B.; Liu, Q. Crack behavior of expanded polystyrene foam-ceramsite composite thermal insulation mortar. *J. Build. Eng.* **2023**, *74*, 106930. [CrossRef]
18. El-Seidy, E.; Sambucci, M.; Chougan, M.; Al-Kheetan, M.J.; Biblioteca, I.; Valente, M.; Ghaffar, S.H. Mechanical and physical characteristics of alkali-activated mortars incorporated with recycled polyvinyl chloride and rubber aggregates. *J. Build. Eng.* **2022**, *60*, 105043. [CrossRef]
19. Meshgin, P.; Xi, Y.; Li, Y. Utilization of phase change materials and rubber particles to improve thermal and mechanical properties of mortar. *Constr. Build. Mater.* **2012**, *28*, 713–721. [CrossRef]
20. Mostofinejad, D.; Aghamohammadi, O.; Bahmani, H.; Ebrahimi, S. Improving thermal characteristics and energy absorption of concrete by recycled rubber and silica fume. *Dev. Built Environ.* **2023**, *16*, 100221. [CrossRef]
21. Wang, J.; Du, B. Experimental studies of thermal and acoustic properties of recycled aggregate crumb rubber concrete. *J. Build. Eng.* **2020**, *32*, 101836. [CrossRef]
22. Zhai, S.; Zhou, X.; Zhang, Y.; Pang, B.; Liu, G.; Zhang, L.; Yang, L.; Liu, Z.; Liu, L. Effect of multifunctional modification of waste rubber powder on the workability and mechanical behavior of cement-based materials. *Constr. Build. Mater.* **2023**, *363*, 129880. [CrossRef]
23. Huang, X.; Pang, J.; Liu, G.; Chen, Y. The influence of equal amplitude high stress repeated loading on the mechanical and deformation characteristics of rubber concrete. *Constr. Build. Mater.* **2021**, *266*, 121135. [CrossRef]
24. Yu, Y.; Jin, Z.; Shen, D.; An, J.; Sun, Y.; Li, N. Microstructure evolution and impact resistance of crumb rubber concrete after elevated temperatures. *Constr. Build. Mater.* **2023**, *384*, 131340. [CrossRef]
25. Davoodi, A.; Esfahani, M.A.; Bayat, M.; Mohammadyan-Yasouj, S.E.; Rahman, A. Influence of nano-silica modified rubber mortar and EVA modified porous asphalt on the performance improvement of modified semi-flexible pavement. *Constr. Build. Mater.* **2022**, *337*, 127573. [CrossRef]
26. Xu, F.; Peng, C.; Zhu, J.; Chen, J. Design and evaluation of polyester fiber and SBR latex compound-modified perlite mortar with rubber powder. *Constr. Build. Mater.* **2016**, *127*, 751–761. [CrossRef]
27. Zhai, S.; Liu, G.; Pang, B.; Liu, C.; Zhang, Z.; Zhang, L.; Liu, L.; Yang, Y.; Liu, Z.; Zhang, Y. Investigation on the influence of modified waste rubber powder on the abrasion resistance of concrete. *Constr. Build. Mater.* **2022**, *357*, 129409. [CrossRef]
28. Luo, T.; Yuan, H.; Wang, Q. Comparison the properties of carbon fiber-based Portland cement and alkali-activated fly ash/slag conductive cementitious composites. *J. Build. Eng.* **2023**, *76*, 107134. [CrossRef]
29. Cheng, Y.; Shen, H.; Zhang, J. Understanding the effect of high-volume fly ash on micro-structure and mechanical properties of cemented coal gangue paste backfill. *Constr. Build. Mater.* **2023**, *378*, 131202. [CrossRef]
30. Shao, R.; Wu, C.; Li, J.; Liu, Z.; Wu, P.; Yang, Y. Mechanical behaviour and environmental benefit of eco-friendly steel fibre-reinforced dry UHPC incorporating high-volume fly ash and crumb rubber. *J. Build. Eng.* **2023**, *65*, 105747. [CrossRef]
31. Zhao, Y.; Chen, X.; Wang, Z.; Zhang, Y.; Leng, Y. An experimental study on the influence of fly ash and crumb rubber on the mechanical property and permeability of Engineered Cementitious Composite (ECC). *J. Build. Eng.* **2023**, *76*, 106998. [CrossRef]
32. Shao, R.; Wu, C.; Li, J.; Liu, Z. Repeated impact resistance of steel fibre-reinforced dry UHPC: Effects of fibre length, mixing method, fly ash content and crumb rubber. *Compos. Struct.* **2023**, *321*, 117274. [CrossRef]
33. Nematzadeh, M.; Hosseini, S.-A.; Ozbakkaloglu, T. The combined effect of crumb rubber aggregates and steel fibers on shear behavior of GFRP bar-reinforced high-strength concrete beams. *J. Build. Eng.* **2021**, *44*, 102981. [CrossRef]
34. Yan, Z.-W.; Bai, Y.-L.; Ozbakkaloglu, T.; Gao, W.-Y.; Zeng, J.-J. Axial impact behavior of Large-Rupture-Strain (LRS) fiber reinforced polymer (FRP)-confined concrete cylinders. *Compos. Struct.* **2021**, *276*, 114563. [CrossRef]
35. Yang, H.; Lu, X.; Gong, M.; Yang, P. Compression-shear performance of steel fiber reinforced rubber concrete. *J. Build. Eng.* **2023**, *75*, 106977. [CrossRef]
36. Xiong, C.; Li, Q.; Lan, T.; Li, H.; Long, W.; Xing, F. Sustainable use of recycled carbon fiber reinforced polymer and crumb rubber in concrete: Mechanical properties and ecological evaluation. *J. Clean. Prod.* **2021**, *279*, 123624. [CrossRef]
37. Su, Q.; Xu, J. Durability and mechanical properties of rubber concrete incorporating basalt and polypropylene fibers: Experimental evaluation at elevated temperatures. *Constr. Build. Mater.* **2023**, *368*, 130445. [CrossRef]
38. Alguhi, H.; Tomlinson, D. Crack behaviour and flexural response of steel and chopped glass fibre-reinforced concrete: Experimental and analytical study. *J. Build. Eng.* **2023**, *75*, 106914. [CrossRef]

39. Kumari, G.J.; Mousavi, S.S.; Bhojaraju, C. Influence of thermal cycles and high-temperature exposures on the residual strength of hybrid steel/glass fiber-reinforced self-consolidating concrete. *Structures* **2023**, *55*, 1532–1541. [CrossRef]
40. *GB 1334-1999*; Slag Portland Cement, Pozzolanic Portland Cement and Fly Ash Portland Cement. National Quality Supervision Bureau: Beijing, China, 1999.
41. *GB/T 208-2014*; Test method of Cement Density. National Quality Supervision Bureau: Beijing, China, 2014.
42. *GB/T 175-1999*; Portland Cement and Ordinary Portland Cement. National Quality Supervision Bureau: Beijing, China, 1999.
43. *GB/T 14684-2022*; Construction-Use Sands. National Quality Supervision Bureau: Beijing, China, 2022.
44. *JG/T 223-2017*; Polycarboxylate Superplasticizers. National Quality Supervision Bureau: Beijing, China, 2017.
45. Aziz, F.N.A.A.; Bida, S.M.; Nasir, N.A.M.; Jaafar, M.S. Mechanical properties of lightweight mortar modified with oil palm fruit fibre and tire crumb. *Constr. Build. Mater.* **2014**, *73*, 544–550. [CrossRef]
46. Benazzouk, A.; Mezreb, K.; Doyen, G.; Goullieux, A.; Quéneudec, M. Effect of rubber aggregates on the physico-mechanical behaviour of cement–rubber composites-influence of the alveolar texture of rubber aggregates. *Cem. Concr. Compos.* **2003**, *25*, 711–720. [CrossRef]
47. *GB/T 2419-2005*; Determination Method of Fluidity of Cement Mortar. National Quality Supervision Bureau: Beijing, China, 2005.
48. *GB/T 17671-2020*; Cement Mortar Strength Test Method (ISO). National Quality Supervision Bureau: Beijing, China, 2020.
49. *JGJ/T 70-2009*; Test Method for Basic Properties of Building Mortar. National Quality Supervision Bureau: Beijing, China, 2009.
50. *GB/T 1843-2008*; Determination of Impact Strength of Plastic Cantilever Beams. National Quality Supervision Bureau: Beijing, China, 2008.
51. *GB/T 6342-1996*; Determination of Linear Dimension of Foamed Plastics and Rubber. National Quality Supervision Bureau: Beijing, China, 1996.
52. *GB/T 10294-2008*; Determination of Steady-State Thermal Resistance and Related Characteristics of Thermal Insulation Materials. National Quality Supervision Bureau: Beijing, China, 2008.
53. Cao, W.; Wang, A.; Yu, D.; Liu, S.; Hou, W. Establishment and implementation of an asphalt pavement recycling decision system based on the analytic hierarchy process. *Resour. Conserv. Recycl.* **2019**, *149*, 738–749. [CrossRef]
54. Li, Y.; Mu, J.; Hao, J.; Liu, Y.; Jiang, X.; Luo, X. Research on the particle characteristics of manufactured sands affecting the flow ability of fresh mortar. *Constr. Build. Mater.* **2023**, *382*, 131287. [CrossRef]
55. Abd-Elaty, M.A.A.; Ghazy, M.F.; Khalifa, O.H. Mechanical and thermal properties of fibrous rubberized geopolymer mortar. *Constr. Build. Mater.* **2022**, *354*, 129192. [CrossRef]
56. Guler, S.; Akbulut, Z.F. Workability, physical & mechanical properties of the cement mortars strengthened with metakaolin and steel/basalt fibers exposed to freezing-thawing periods. *Constr. Build. Mater.* **2023**, *394*, 132100.
57. Feng, W.; Tang, Y.; Zhang, Y.; Qi, C.; Ma, L.; Li, L. Partially fly ash and nano-silica incorporated recycled coarse aggregate based concrete: Constitutive model and enhancement mechanism. *J. Mater. Res. Technol.* **2022**, *17*, 192–210. [CrossRef]
58. Fang, Z.; Luo, Y.; Chen, H.; Gao, Y.; Yang, W.; Wang, C. Research on mechanical properties and hydration characteristics of ultra-high performance concrete with high-volume fly ash microsphere. *J. Build. Eng.* **2023**, *78*, 107738. [CrossRef]
59. Li, H.-W.; Wang, R.; Wei, M.-W.; Lei, N.-Z.; Sun, H.-X.; Fan, J.-J. Mechanical properties and hydration mechanism of high-volume ultra-fine iron ore tailings cementitious materials. *Constr. Build. Mater.* **2022**, *353*, 129100. [CrossRef]
60. Li, D.; Zhuge, Y.; Gravina, R.; Mills, J.E. Compressive stress strain behavior of crumb rubber concrete (CRC) and application in reinforced CRC slab. *Constr. Build. Mater.* **2018**, *166*, 745–759. [CrossRef]
61. Li, H.; Long, W.-J.; Khayat, K.H. Efficient recycling of waste rubber in a sustainable fiber-reinforced mortar and its damping and energy dissipation capacity. *Cem. Concr. Compos.* **2023**, *138*, 104963. [CrossRef]
62. Qaidi, S.; Mohammed, A.S.; Ahmed, H.U.; Faraj, R.H.; Emad, W.; Tayeh, B.A.; Althoey, F.; Zaid, O.; Sor, N.H. Rubberized geopolymer composites: A comprehensive review. *Ceram. Int.* **2022**, *48*, 24234–24259. [CrossRef]
63. Chinchillas-Chinchillas, M.J.; Orozco-Carmona, V.M.; Gaxiola, A.; Alvarado-Beltrán, C.G.; Pellegrini-Cervantes, M.J.; Baldenebro-López, F.J.; Castro-Beltrán, A. Evaluation of the mechanical properties, durability and drying shrinkage of the mortar reinforced with polyacrylonitrile microfibers. *Constr. Build. Mater.* **2019**, *210*, 32–39. [CrossRef]
64. Afroughsabet, V.; Biolzi, L.; Ozbakkaloglu, T. Influence of double hooked-end steel fibers and slag on mechanical and durability properties of high performance recycled aggregate concrete. *Compos. Struct.* **2017**, *181*, 273–284. [CrossRef]
65. Uygunoğlu, T.; Topçu, I.B. The role of scrap rubber particles on the drying shrinkage and mechanical properties of self-consolidating mortars. *Constr. Build. Mater.* **2010**, *24*, 1141–1150. [CrossRef]
66. Su, P.; Dai, Q.; Li, M.; Ma, Y.; Wang, J. Investigation of the mechanical and shrinkage properties of plastic-rubber compound modified cement mortar with recycled tire steel fiber. *Constr. Build. Mater.* **2022**, *334*, 127391. [CrossRef]
67. Deng, Z.; Yang, Z.; Pan, X. Synergetic effects of recycled crumb rubber and glass cullet on the engineering properties of geopolymer mortar. *Cem. Concr. Compos.* **2023**, *137*, 104907. [CrossRef]
68. Chen, W.; Xie, Y.; Li, B.; Li, B.; Wang, J.; Thom, N. Role of aggregate and fibre in strength and drying shrinkage of alkali-activated slag mortar. *Constr. Build. Mater.* **2021**, *299*, 124002. [CrossRef]
69. Zhang, J.; Pan, G.; Yan, Y. Early hydration, mechanical strength and drying shrinkage of low-carbon alkali-activated Ti-extracted residues-fly ash cement and mortars. *Constr. Build. Mater.* **2021**, *293*, 123517. [CrossRef]
70. Wang, H.; Long, G.; Xie, Y.; Zeng, X.; Ma, K.; Dong, R.; Tang, Z.; Xiao, Q. Effects of intense ultraviolet irradiation on drying shrinkage and microstructural characteristics of cement mortar. *Constr. Build. Mater.* **2022**, *347*, 128513. [CrossRef]

71. Xiang, J.; Qiu, J.; Zhao, Y.; Zheng, P.; Peng, H.; Fei, X. Rheology, mechanical properties, and hydration of synergistically activated coal gasification slag with three typical solid wastes. *Cem. Concr. Compos.* **2023**, *147*, 105418. [CrossRef]
72. Liu, M.; Lu, J.; Ming, P.; Yin, Y. Study of fracture properties and post-peak softening process of rubber concrete based on acoustic emission. *Constr. Build. Mater.* **2021**, *313*, 125487. [CrossRef]
73. Najim, K.; Hall, M. Mechanical and dynamic properties of self-compacting crumb rubber modified concrete. *Constr. Build. Mater.* **2012**, *27*, 521–530. [CrossRef]
74. El Wardi, F.Z.; Ibaaz, K.; Bouyahyaoui, A.; Cherkaoui, M.; Ouaki, B.; Oubenmoh, S. Thermomechanical characterization and thermal simulation of a new multilayer mortar and a light-weight pozzolanic concrete for building energy efficiency. *Constr. Build. Mater.* **2022**, *346*, 128479.
75. Awoyera, P.O.; Akinrinade, A.D.; de Sousa Galdino, A.G.; Althoey, F.; Kirgiz, M.S.; Tayeh, B.A. Thermal insulation and mechanical characteristics of cement mortar reinforced with mineral wool and rice straw fibers. *J. Build. Eng.* **2022**, *53*, 104568. [CrossRef]
76. Guardia, C.; Barluenga, G.; Palomar, I.; Diarce, G. Thermal enhanced cement-lime mortars with phase change materials (PCM), lightweight aggregate and cellulose fibers. *Constr. Build. Mater.* **2019**, *221*, 586–594. [CrossRef]